Acta Crystallographica Section D
Biological Crystallography
ISSN 0907-4449

Dimeric Sfh3 has structural changes in its binding pocket that are associated with a dimer–monomer state transformation induced by substrate binding

Ye Yuan,[a,b] Wei Zhao,[a,b] Xiao Wang,[a,b] Yongxiang Gao,[a,b] Liwen Niu[a,b]* and Maikun Teng[a,b]*

[a]Hefei National Laboratory for Physical Sciences at Microscale, School of Life Sciences, University of Science and Technology of China, 96 Jinzhai Road, Hefei, Anhui 230026, People's Republic of China, and [b]Key Laboratory of Structural Biology, Chinese Academy of Sciences, 96 Jinzhai Road, Hefei, Anhui 230027, People's Republic of China

Correspondence e-mail: lwniu@ustc.edu.cn, mkteng@ustc.edu.cn

Received 18 June 2012
Accepted 8 November 2012

PDB Reference: dimeric Sfh3, 4fmm

Phosphorylated derivatives of phosphatidylinositol (PtdIns), also called phosphoinositides (PIPs), are basic components of membrane-associated signalling systems. A family of PtdIns-transfer proteins (PITPs) called the Sec14 family have been predicted to form a set of functional modules that can sense different types of lipid metabolism and transmit the information to the PIP signalling system. In eukaryotic cells, the Sec14 family exhibits a wide diversity of activity, but the structural basis of this diversity remains unclear. In the present study, the dimeric structure of Sfh3 (Sec14 family homologue 3 in yeast) is reported for the first time and differs from the Sec14 proteins reported to date, all of which are monomeric. Some variations in the binding pocket of Sfh3 were observed and the dimer interface was identified and proposed to provide a link between dimer–monomer state changes and PtdIns binding. Together, these structural changes and the oligomeric state transformation of Sfh3 support ideas of diversity within the Sec14 family and provide some new clues to function.

1. Introduction

In eukaryotic cells, the compartmentalization of membranes (including plasma and subcellular membranes) is fundamental to various biochemical reactions that occur within the proximity of membranes in a spatial and temporal manner (Schaaf *et al.*, 2008). Membranes in general are specialized by their two basic components: membrane proteins and lipids. According to the classic 'fluid mosaic model' (Singer & Nicolson, 1972), lipids in membranes act as liquids. Their composition is maintained and regulated by membrane-associated signalling systems. These signalling systems utilize various 'functional modules' such as membrane transport and recognition, lipid metabolism, sensing of lipid molecules and so on for compartmentalization (Lemmon, 2008).

Phosphorylated derivatives of phosphatidylinositol (PtdIns), also called phosphoinositides (PIPs), function as elementary components of membrane-associated signalling systems (Di Paolo & De Camilli, 2006). *In vitro* studies have shown that the production of individual PIPs is catalyzed directly by specific PtdIns kinases (Fruman *et al.*, 1998). However, increasing evidence points to the weak activity of PtdIns kinases in biological systems and the complexity of PIP signal synthesis *in vivo* (Strahl & Thorner, 2007). Among lipid-transfer proteins, the PtdIns/phosphatidylcholine (PtdCho) transfer proteins (PITPs) play significant roles in PIP signal synthesis and regulation (Ile *et al.*, 2006).

In *Saccharomyces cerevisiae* the major PITP is Sec14, which has been shown to link phospholipid metabolism to vesicle formation on TGN (trans-Golgi network) membranes in previous studies (Salama *et al.*, 1990; Kearns *et al.*, 1997). However, recent studies have revised the role of Sec14 from a lipid carrier to a component in the regulation of PtdIns 4-OH kinase activities for PIP signalling (Schaaf *et al.*, 2008; Bankaitis *et al.*, 2010). In particular, Sec14 plays an intermediate role as a PtdCho sensor and a PtdIns-presenting nanoreactor based on its ability to bind to both PtdIns and PtdCho.

Sec14 is one of about 1500 proteins containing similar domains, with Sec14 as their prototype, which form the eukaryotic Sec14 protein family as annotated in the NCBI database (Phillips *et al.*, 2006). The roles of these proteins in various cellular activities stem from studies associating the dysfunction of human Sec14 proteins with a number of diseases (Ouachi *et al.*, 1995; Maw *et al.*, 1997; Cichowski & Jacks, 2001). The biological significance of the apparent redundancy in Sec14 proteins is an interesting subject for investigation. Within the PIP signalling system, the Sec14 family of proteins are predicted to act as functional modules that sense different types of lipid metabolism (not only PtdCho) and transmit the information down the PIP signalling cascade (Bankaitis *et al.*, 2010; Schaaf *et al.*, 2011). Therefore, it is presumed that substrate binding in Sec14 proteins may be conserved for PtdIns (or PIPs) but may be variable for other substrates.

There are five Sec14 homologues (Sfh1–5) in yeast, which share 21–64% identity with Sec14 (Griac *et al.*, 2006). However, with the exception of Sfh1, which is the closest Sec14 homologue with 64% identity, they exhibit significant PtdIns-transfer activity but no PtdCho-transfer activity. None of them has been shown to compensate the function of Sec14 independently *in vivo* (Li *et al.*, 2000). Sfh3, which shares 23% identity with Sec14 (van den Hazel *et al.*, 1999), displays similar PtdIns- and PtdCho-binding activities *in vitro* as other Sfh proteins (with the exception of Shf1). In contrast to the wide subcellular distribution of Sec14, Sfh3 is exclusively found in lipid particles and microsomes in C-terminal yEGFP fusion experiments *in vivo* (Li *et al.*, 2000; Schnabl *et al.*, 2003). Until now, Sfh3 has not been well characterized. Studies have reported that the loss of Sfh3 can alter the sterol composition of membranes (Griac *et al.*, 2006). Deletion of the *sfh3* gene increases the sensitivity to azole antifungals and the double mutant *sfh3*Δ*sfh4*Δ shows a novel hypersensitivity to an extensive range of drugs such as mutagens, inhibitors of protein synthesis *etc.* (van den Hazel *et al.*, 1999). All of these characteristics highlight unique features of Sfh3 that differentiate it from other Sec14 proteins.

In the present study, we report the structure of Sfh3, revealing it to be a homodimer; this is in contrast to all other known Sec14 proteins, which are monomeric. In the structure of Sfh3, a helix (α7) forming one side of the lipid-binding pocket differs drastically from the other Sec14 proteins and reflects unique changes. This modified α7 helix and the amino-acid substitutions in some residues pointing into the interior together change the shape of the pocket, making it the largest of the Sec14 domains. We also identify the dimer interface of Sfh3, which is formed from a highly conserved region together with the altered helix α7, indicating that dimerization and substrate binding are interlinked by the unique dimer interface of Sfh3. This may also provide the structural basis for a substrate-binding-induced dimer–monomer state change. These structural features are consistent with the predicted roles of Sec14 protein family members and provide some new insights into their function.

2. Materials and methods

2.1. Cloning, expression and purification

We cloned the gene (gene ID 855490) encoding full-length Sfh3 (41 kDa) by PCR from *S. cerevisiae* genomic DNA. The PCR product was digested and inserted into the p22b vector (derived from pET22b, Novagen, USA) between *Nde*I and *Xho*I sites to add a His_6 tag at the C-terminus (LEHHHHHH) of Sfh3. We also created mutations of Sfh3 using the MutanBEST kit (Takara, Japan) following the manufacturer's protocol. The accuracy of the constructs was confirmed by DNA sequencing.

Escherichia coli Arctic Express (DE3) RIL cells (Agilent, USA) were transformed with the plasmid to overexpress the recombinant Sfh3. The cells were cultured in LB medium with 50 µg ml^{-1} ampicillin at 310 K until the $OD_{600\,nm}$ reached 0.6–0.8. Protein expression was then induced with 0.25 m*M* β-D-1-thiogalactopyranoside (IPTG) for 20 h at 289 K. After centrifugation, the cells were resuspended and lysed in buffer *A* (20 m*M* Tris–HCl pH 7.0, 500 m*M* NaCl, 2 m*M* EDTA, 2 m*M* Triton X-100).

The purification of Sfh3 generally consisted of two steps: Ni^{2+}-affinity chromatography followed by a second step in which the preliminary product was concentrated for gel filtration. When purified using HiLoad Superdex 75 16/600 (GE Healthcare, USA) in buffer *B* (20 m*M* Tris–HCl pH 7.0, 200 m*M* NaCl, 1 m*M* β-mercaptoethanol), Sfh3 eluted as a single peak with a size corresponding to a dimer. The purified protein was then concentrated to 20–30 mg ml^{-1} and stored in buffer *C* (20 m*M* Tris–HCl pH 7.0, 140 m*M* NaCl, 1 m*M* β-mercaptoethanol) at 193 K.

A selenomethionine derivative of Sfh3 (Se-Sfh3) was overexpressed in the same competent cells as native Sfh3 but in M9 medium, based on a methionine-biosynthesis inhibition method (improved from Walsh *et al.*, 1999; see Supplementary Material[1]). The purification of Se-Sfh3 and the Sfh3 mutants followed the same protocol as used for native Sfh3.

2.2. Crystallization, data collection and structure determination

Preliminary screening of Sfh3 for crystallization was performed with a Mosquito liquid-handling robot (TTP LabTech, UK) using Crystal Screen, Index, SaltRX, Grid

[1] Supplementary material has been deposited in the IUCr electronic archive (Reference: BE5212). Services for accessing this material are described at the back of the journal.

Table 1
Data-collection and refinement statistics.

Values in parentheses are for the outer shell.

	Native	SeMet
Data-collection statistics		
Wavelength (Å)	0.97915	0.97917
Space group	$C222_1$	$C222_1$
Unit-cell parameters	a = 76.18, b = 76.91, c = 294.96, $\alpha = \beta = \gamma$ = 90.00	a = 76.81, b = 77.07, c = 293.76, $\alpha = \beta = \gamma$ = 90.00
Resolution range (Å)	50.00–2.34 (2.38–2.34)	50.00–2.90 (2.95–2.90)
No. of reflections	226596	198620
No. of unique reflections	35651	19913
$R_{\rm merge}$† (%)	5.7 (10.5‡)	12.2 (46.5)
$\langle I/\sigma(I)\rangle$	19.25 (12.28)	30.19 (7.68)
Multiplicity	6.4	10.0
Completeness (%)	95.7 (76.0)	99.5 (100.0)
Refinement statistics		
Resolution range (Å)	50.00–2.34	
No. of reflections (work/test)	33809/1781	
No. of non-H atoms	5519	
Protein	5191	
Water	271	
Others	57 [9 glycerols, 3 Mg ions]	
$R_{\rm work}$§/$R_{\rm free}$¶ (%)	21.7/26.4	
R.m.s.d.††		
Bond lengths (Å)	0.008	
Bond angles (°)	1.10	
Average B factor (Å^2)	23.12	
Ramachandran plot (%)		
Favoured	98.7	
Outliers	0	

† $R_{\rm merge} = \sum_{hkl}\sum_i |I_i(hkl) - \langle I(hkl)\rangle| / \sum_{hkl}\sum_i I_i(hkl)$, where $I_i(hkl)$ is the intensity of an observation and $\langle I(hkl)\rangle$ is the mean value for its unique reflection; summations are over all reflections. ‡ The value for the highest resolution shell is limited by the completeness (<50%). § R factor = $\sum_{hkl} ||F_{\rm obs}| - |F_{\rm calc}|| / \sum_{hkl} |F_{\rm obs}|$, where $F_{\rm obs}$ and $F_{\rm calc}$ are the observed and calculated structure-factor amplitudes, respectively. Summation includes all reflections used in the refinement. ¶ Free R factor calculated with 5% of the data excluded from the refinement. †† Root-mean-square deviation from ideal values.

Screen (Hampton Research, USA) and ProPlex (Molecular Dimensions, UK). Tiny plate-shaped crystals of Sfh3 appeared after a few days under several conditions. Two conditions, Crystal Screen condition No. 18 and ProPlex condition No. 1.43, were selected for optimization using the hanging-drop vapour-diffusion method. Crystals with the appearance of long three-dimensional rods with good diffraction quality finally grew after 3 d using a mixture of the two conditions in a 1:4(v:v) ratio at 287 K. Good crystals of Se-Sfh3 appeared under the same conditions as used for native Sfh3.

Before data collection, the crystals were briefly soaked in a cryoprotectant solution consisting of reservoir solution supplemented with 25%(v/v) glycerol. X-ray diffraction data for native Sfh3 and Se-Sfh3 were collected on beamline 17U1 of Shanghai Synchrotron Radiation Facility (SSRF), People's Republic of China using a Jupiter CCD detector at 100 K. A 2.34 Å resolution X-ray diffraction data set was collected from one native Sfh3 crystal. A selenium single-wavelength (λ = 0.97917 Å) anomalous dispersion (SAD) data set was collected to 2.90 Å resolution from one Se-Sfh3 crystal. All diffraction data were processed and scaled with *HKL*-2000 (Otwinowski & Minor, 1997).

We used the SAD method for phasing. Using the *PHENIX* program package, eight of the ten predicted Se sites were located and the initial phases were calculated (Adams *et al.*, 2002). In one asymmetric unit, 85% of the residues were built automatically using *phenix.autobuild* in the *PHENIX* program package and the remaining parts were built manually using the *Coot* program (Emsley & Cowtan, 2004). The model was then refined against the 2.34 Å resolution native data set using alternating cycles of *REFMAC*5 (Murshudov *et al.*, 2011) and *Coot*. Data-processing and structure-determination statistics are tabulated in Table 1.

2.3. Construction of the 'closed' model of Sfh3 and docking of Sfh3 with PtdIns

The 'closed' model of Sfh3 was constructed in two steps. Firstly, a preliminary model was built by *MODELLER* using the *ESyPred3D* server (Lambert *et al.*, 2002) with the structure of Sfh1 with PtdIns (PDB entry 3b7n; Schaaf *et al.*, 2008) as a template for *in silico* substitutions. Secondly, this model was refined using the *Rosetta* 3.3 program (Leaver-Fay *et al.*, 2011) to minimize the *Rosetta* score, a parameter that measures the quality of the model. The refined model of Sfh3 was then used for structural comparison, volume calculation of the binding pocket and substrate docking.

The structure of the PtdIns monomer was modified by *Open Babel* before substrate docking (O'Boyle *et al.*, 2011). PtdIns was computationally docked to the 'closed' Sfh3 model using *RosettaLigand* (Davis & Baker, 2009) with *FROG* (Leite *et al.*, 2007) to generate an ensemble of substrate conformations. For this docking, over 1000 ligand-docking simulations were calculated and the lowest energy decoy was chosen as the best result for structural discussion.

2.4. Incubation experiments of Sfh3 with PtdIns

In these experiments, high-resolution gel-retardation chromatography (Superdex 75 10/600; GE Healthcare, USA) was used to detect changes in the oligomeric state in solution after pre-equilibration with buffer *P* consisting of 50 m*M* Tris–HCl, 150 m*M* NaCl pH 7.0. PtdIns (Sigma, Germany) was dissolved directly in ddH_2O by ultrasonication and suitable heating (to about 315 K). PtdIns (2 m*M*) was added dropwise to a solution consisting of 100 µ*M* protein (Sfh2, Sfh3 or Sfh4) until the substrate:protein monomer ratio reached about 5:1. After incubation for 1–2 h at 297 K, the sample was concentrated to 100 µl and centrifuged for loading. The working flow rate was 0.5 ml min^{-1} and the test was repeated twice for each protein sample.

3. Results and discussion

3.1. Crystal structure of Sfh3

In previous studies, two conformations of Sec14 proteins have been determined (Bankaitis *et al.*, 2010): an 'open' conformation found in apo proteins (such as Sec14; PDB entry 1aua; Sha *et al.*, 1998) and a 'closed' conformation in proteins with substrates (such as Sfh1 with PtdIns and PtdCho; PDB

entries 3b7n and 3b7q; Schaaf *et al.*, 2008). We observed that there were no lipid molecules in the electron-density map for Sfh3. In addition, structural alignment using *DALI* (Holm & Rosenström, 2010) also revealed that the Sfh3 structure was most similar to the open conformation of Sec14 (Z score of >18.0), confirming that the crystal structure of Sfh3 is in an open conformation.

The overall structure of Sfh3 consists of 11 α-helices, nine β-strands and seven 3_{10}-helices. Like the other yeast Sec14 proteins, Sfh3 has two major domains: the N- and C-domains (Fig. 1*a*). The N-domain is distinguished by a tripod-like motif consisting of three helices: α1, α2–α3 (regarded as a fractured helix) and α4. Unlike Sec14, Sfh3 contains an inserted hairpin motif (β2–loop–β3) between α1 and α2–α3 which stretches out from the overall framework of the Sfh3 structure (Fig. 1*b*). The C-domain, which is also known as the Sec14 domain, has a 'baseball-glove' shape. It consists of five α-helices (α5–α9), five β-strands (β4–β8) and six 3_{10}-helices (η2–η7). The five β-strands, which are arranged in the order β4–β5–β6–β7–β8, form a central β-sheet constituting the binding-pocket floor. One side of the pocket, formed by α8–η4 and α9, is highly conserved and is called the gating helix (Fig. 1*b*), but the other side (α6 and α7) exhibits significant changes (discussed in later sections).

Besides the two major domains, Sfh3 has several exclusive inserted elements, including the β2–loop–β3, a long nonconserved α-helix (α10) and other motifs, a long loop at the N-terminus (N-loop), α11 and the β1–β9 sheet (Figs. 1*b* and 1*c*). Except for the β2–loop–β3 motif, these all extend around the β-sheet floor of the binding pocket. The additional motifs interact with the N-domain and Sec14 domain *via* hydrogen bonds [*e.g.* Ile25/Leu26 (N-loop) to Tyr150 (β4), Tyr315 (α10) to Ala83/Thr86 (α2) and Asn320 (α10) to Glu79 (α2)] and interact with themselves *via* various other interactions. In this way, these unique motifs of Sfh3 wrap the binding pocket like a 'woven net', which stabilizes the hydrophobic pocket and preserves the potential energy for lipid binding.

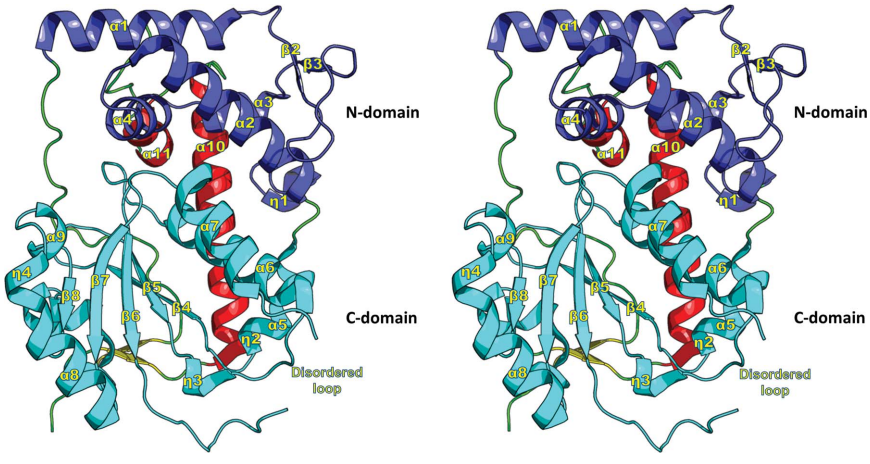

Figure 1
Overall three-dimensional structure of the Sfh3 monomer. The molecule is shown in stereo, with the N-domain and the C-domain coloured blue and cyan, respectively. The secondary structures are also labelled.

3.2. Structural changes in the binding pocket

As shown in Fig. 2(*a*), the most marked change in Sfh3 is in α7, which forms part of the binding pocket. Unlike its counterparts in other Sec14 proteins, which bend towards the pocket, α7 bends away from the pocket. Interestingly, residues 211–217 have no density in the electron-density map and their absence from the model leaves an apparent gap in the 'wall' of the pocket where a helix is expected. To investigate this, we modelled the missing residues 211–217 using *JiffLoop* in *MolProbity* (Chen *et al.*, 2010; see Supplementary Material). The prediction suggested a significant spatial difference of at least 6.7 Å, as shown in Fig. 2(*b*), changing the shape of the binding pocket.

We further constructed a 'closed' model of Sfh3 for structural comparison (§2.3). Two factors support the rationality of this model: (i) the overall structural rigidity of the open and closed conformations, apart from the gating helix (Ryan *et al.*, 2007), and (ii) the strict sequence conservation of the gating helix between Sfh3 and other Sec14 proteins, especially Sfh1. The closed model displays some variations in specific residues. In Sfh1, Phe233 (from the gating helix) interacts with Lys197 (from α8) at a distance of 3.6 Å, which seals the binding pocket, as shown in Fig. 2(*c*). Several other residues from the gating helix and α8 are close to each other, forming hydrophobic interactions that stabilize the closed conformation (Schaaf *et al.*, 2008). In contrast, in the closed model of Sfh3 the distance between Phe259 and Lys223 (the counterparts of Phe233 and Lys197 in Sfh1) is about 7.8 Å and they cannot form any effective interaction to close the pocket. Structural elements of the hydrophobic interactions in Sfh1 are also lost completely in Sfh3 because of the gap involving residues 211–217 (Fig. 2*c*).

3.3. Volume of the binding pocket

Changes in α7 of Sfh3 result in a large increase in the volume of the substrate-binding pocket. However, other factors also contribute to the increase in volume. Two factors can affect the size of the pocket: the spatial location of the C^{α} backbone in the binding pocket and the size of the residue side chains that point into the pocket interior. In Sec14, large residues such as Tyr111, Tyr122, Tyr151, Met177, Glu202 and Phe212 are distributed along the binding pocket. Acting as a series of 'mechanical arms' extending into the interior of the pocket, they narrow the pocket volume and control substrate cycling into and out of the pocket interior (Schaaf *et al.*, 2011; Supplementary Fig. 1*a*). However, in Sfh3 these large residues are substituted by residues with smaller side chains. For example, Tyr111 is substituted by Ile147, Tyr122 by Leu158, Tyr151 by Leu181, Met177 by Ile199 and Phe212 by Ala240. These changes rearrange the distribution of

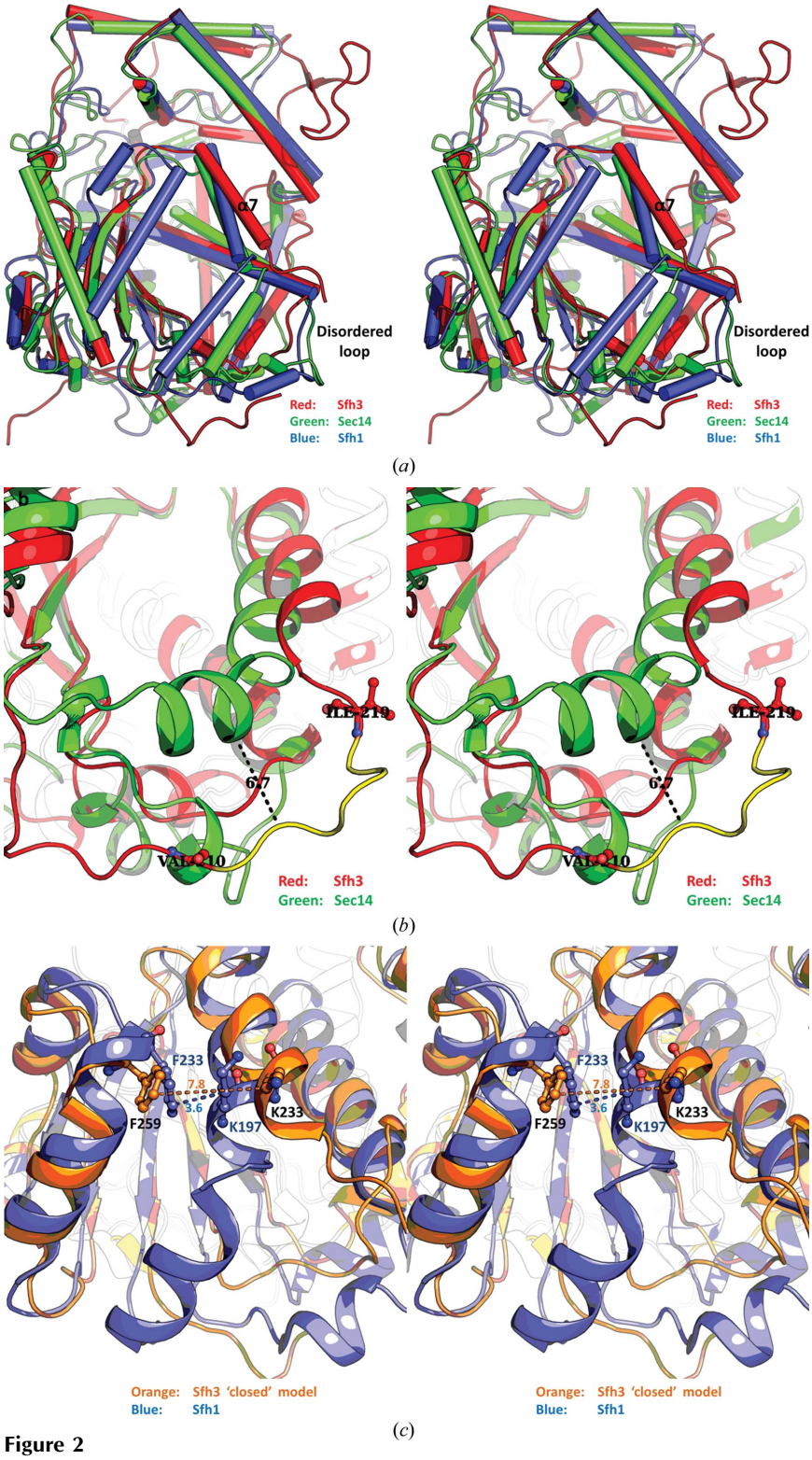

Figure 2
(*a*) Stereoview of the Sfh3 monomer with known structures of Sec14 and Sfh1. The structure of Sfh3 is coloured red and is compared with the structures of Sec14 in an open conformation (green; PDB entry 1aua) and of Sfh1 in a closed conformation (blue; PDB entry 3b7n). All helices are shown as cylinders. Major changes in Sfh3 (α7) and the disordered loop are marked. (*b*) Stereo representation of the structural alignment between Sec14 (green; PDB entry 1aua) and an Sfh3 model (red) in which the gap of the pocket was filled using *JiffLoop* (coloured yellow). (*c*) Stereoview of the structural alignment between the closed model of Sfh3 (orange) and Sfh1 (blue; PDB entry 3b7n). The residues Phe233, Lys197 (in Sfh1), Phe259 and Lys223 (in the closed model of Sfh3) are shown as sticks and the relevant distances (Phe233–Lys197 and Phe259–Lys223) are indicated.

the residue side chains in the binding-pocket interior and increase the cavity correspondingly (Supplementary Fig. 1*b*).

Thus, the displacement of α7 and substitution of large residues results in an increase in the pocket volume of Sfh3, which has the largest volume of all structures of Sec14 domains reported to date. To describe this feature quantitatively, we used the volume-calculating tool 3*V* (Voss & Gerstein, 2010). As Table 2 and Supplementary Fig. S2 show, the calculated pocket volume of Sfh3 is about twice as large as those of others in both the open and the closed conformations. The large binding pocket may allow Sfh3 to bind some new substrates, such as larger lipids (steroids, multi-tailed phospholipids *etc.*), which is consistent with the hypothesis of the diversity within the Sec14 family.

3.4. The dimer interface is close to the binding pocket

Sfh3 exists as a dimer in solution in the ligand-free state, as mentioned in §2.1. Although the Sfh3 dimer is quite stable in various buffers, we wanted to exclude the possibility that the dimer might be an artefact of high protein concentration. Therefore, we tested the oligomeric state of a series of Sfh3 samples at different concentrations: 75, 38 and 13 μ*M*. The peak profiles of high-resolution size-exclusion chromatography show that all of the samples elute as stable dimers in solution, even at concentrations lower than 15 μ*M* (Fig. 6*b*). At such low concentrations, the average static intermolecular distance of the Sfh3 molecule (calculated at about 2000 Å for a monomer) is much larger than the radius of the monomer (about 30 Å), suggesting that non-specific intermolecular interactions cannot be the major factor in dimerization.

Sfh3 crystallizes with two structurally similar molecules (monomers *A* and *B*) in the asymmetric unit. Structural alignment of the two molecules shows that the C^{α} atoms of 324 residues can be superimposed with an r.m.s.d. (root-mean-square deviation) of 0.28 Å (*FATCAT*; http://fatcat.burnham.org/fatcat/; Ye & Godzik, 2003). From the overall structure, we observed two possible interfaces which would lead to two alternative dimers: dimer I (Fig. 3*a*) and dimer II (Fig. 3*b*). To determine the dimer interface, we used the *PDBePISA* server (Krissinel & Henrick, 2007; http://www.ebi.ac.uk/msd-srv/

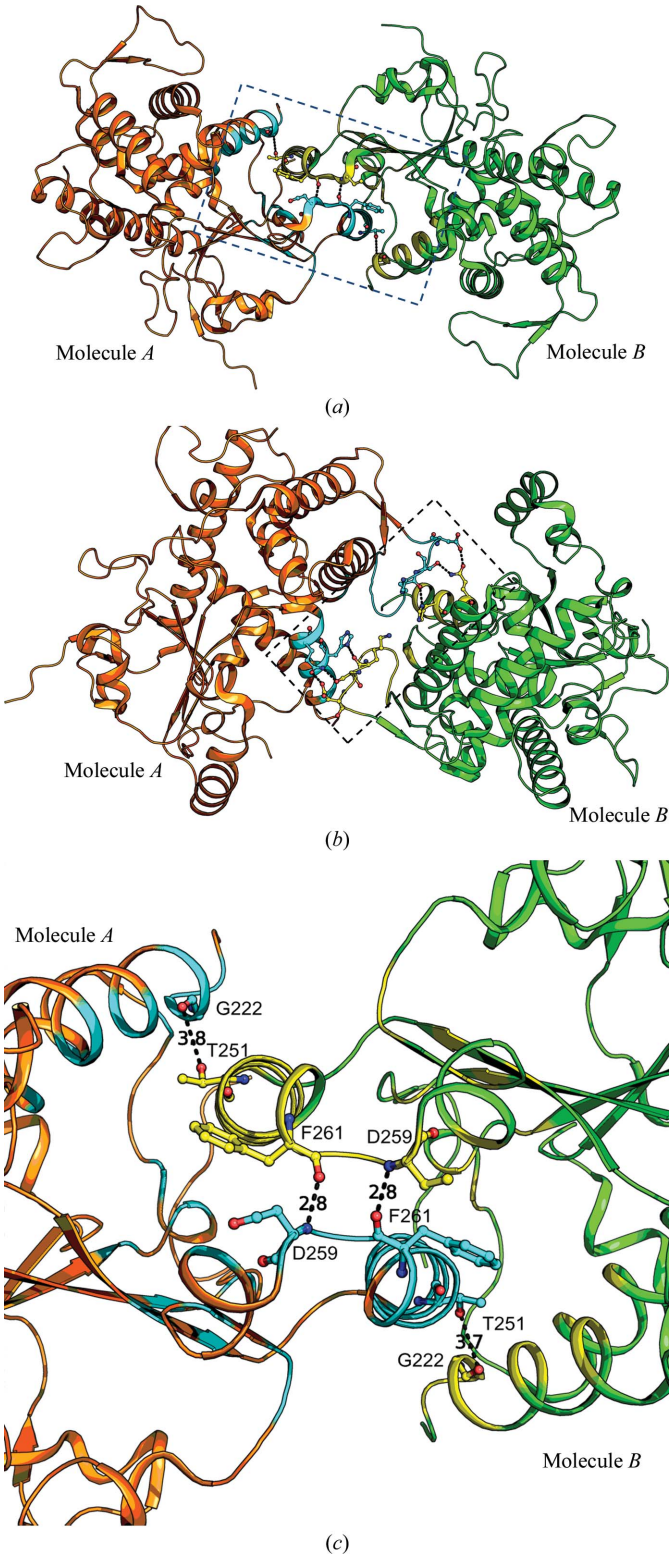

Figure 3
(*a*) Ribbon representation of Sfh3 dimer I. The two molecules are coloured orange (molecule *A*) and green (molecule *B*) and the regions involved in the dimer interaction are coloured cyan (for molecule *A*) and yellow (for molecule *B*). (*b*) The ribbon representation of the Sfh3 dimer II within the interface of the dimer is coloured cyan (for molecule *A*) and yellow (for molecule *B*). (*c*) Representations of the interactions in the dimer interface in dimer I. Residues forming hydrogen bonds are shown in stick form.

Table 2
Calculation of the volume of the binding pocket.

The PDB codes are as follows: Sec14, 1aua (Sha *et al.*, 1998); Sfh1, 3b7n (Schaaf *et al.*, 2008); human α-TTP, open conformation, 1oiz; human α-TTP, closed conformation, 1r5l (Meier *et al.*, 2003).

Open conformation			Closed conformation		
Protein	Volume (Å^3)	Surface area (Å^2)	Protein	Volume (Å^3)	Surface area (Å^2)
Sfh3	3384	1970	Sfh3, closed model	1613	1053
Sec14	1849	1287	Sfh1	798	572
Hs α-TTP, open	1530	1030	Hs α-TTP, closed	587	433

prot_int/pistart.html). The results of these interface and assembly calculations are tabulated in Table 3. As shown in Table 3, the buried surface area upon dimerization of dimer I is 5146.2 Å^2 and the value of Δ^iG (the solvation free-energy gain upon formation of the interface) is -27.9 kcal mol^{-1}, with a Δ^iG *P*-value of 0.005. The closeness of the latter value to zero suggests strong hydrophobicity of the dimer I interface, implying that it is an interaction-specific dimer rather than an artefact of crystal packing. All of the results of the *PISA* analysis were consistent with Sfh3 being a dimer in solution and in the crystals. Based on these results, we preliminarily conclude that Sfh3 is a dimer in the ligand-free state and that the dimer interface corresponds to that in dimer I.

Interaction analysis using *LIGPLOT* (Wallace *et al.*, 1996) revealed details of the dimer interface (Supplementary Fig. S3). Significantly, the interface of dimer I seems to be stabilized predominantly by hydrophobic interactions rather than hydrogen bonds (Fig. 3*c*). In this dimer interface, α7 from one molecule of dimer I interacts with the gating helix from the other molecule, establishing a four-α-helix motif (two gating helices and two α7 helices; Fig. 3*c*). However, in contrast to dimer I, dimer II has an interface that is much smaller and is only stabilized by six pairs of hydrogen bonds (Fig. 3*b*). Significant hydrophobic interactions are not evident in dimer II.

Although all of the results of the structural analysis support dimer I as the relevant form in solution, the possibility of dimer II still has to be excluded. Therefore, we designed several mutations to disrupt the hydrogen bonds in dimer II and finally constructed four mutants for expression and purification (Supplementary Fig. S4). None of the mutants displayed any changes in their dimeric state in solution in the absence of PtdIns, indicating that these residues did not contribute to the main interactions for dimer stabilization. This result indicates that dimer II is not relevant and strengthens the validity of dimer I, although there is not a strict either/or relationship.

3.5. Intrinsic features of the dimer interface embedded in the sequence

As discussed above, we have identified a unique dimer interface in Sfh3. Interestingly, we note that the two structural elements of the interface, the gating helix and α7, exist in all

Table 3
PISA analyses of the two dimer-conformation models of Sfh3 (dimer I and dimer II).

(*a*) Interface summary (dimer I).

Structure 1			Structure 2							
Range	$^{i}N_{at}$†	$^{i}N_{res}$‡	Range	$^{i}N_{at}$	$^{i}N_{res}$	Symmetry operator	Interface area (Å^2)	$\Delta^{i}G$§ (kcal mol^{-1})	$\Delta^{i}G$ *P*-value¶	CSS††
B	116	35	*A*	120	37	*x*, *y*, *z*	1090	−27.9	0.005	0.406

(*b*) Interface summary (dimer II).

Structure 1			Structure 2							
Range	$^{i}N_{at}$	$^{i}N_{res}$	Range	$^{i}N_{at}$	$^{i}N_{res}$	Symmetry operator	Interface area (Å^2)	$\Delta^{i}G$ (kcal mol^{-1})	$\Delta^{i}G$ *P*-value	CSS
A	73	19	*B*	69	18	$x - 1/2$, $y - 1/2$, z	614	−2.7	0.831	0.000

(*c*) Assembly summary. Formula $A_2a_9b_3$. Composition AB[GOL]$_9$[MG]$_3$.

Multimeric state‡‡	Surface area (Å^2)	Buried area (Å^2)	ΔG^{int}§§ (kcal mol^{-1})	ΔG^{diss} (kcal mol^{-1})	$T\Delta S^{diss}$¶¶ (kcal mol^{-1})	Symmetry number
2	29545	5146	−59.1	19.8	13.7	2

† The number of interfacing atoms in the corresponding structure. ‡ The number of interfacing residues in the corresponding structure. § The solvation free-energy gain upon formation of the interface, which corresponds to hydrophobic interfaces, or positive protein affinity. ¶ The *P*-value of the observed solvation free-energy gain. When the value is close to its limiting case $P = 0$, it indicates interfaces with surprising hydrophobicity, implying that the interface surface may be interaction-specific. The closer to 0 the value is, the more interaction-specific the interface may be. †† The complexation significance score (0–1), which indicates how significant for assembly formation the interface is. ‡‡ The total number of macromolecular chains in the assembly. §§ The solvation free-energy gain upon formation of the assembly. ¶¶ The free energy of assembly dissociation; assemblies with $\Delta G^{diss} > 0$ are thermodynamically stable.

known structures of Sec14 proteins. As a crucial element for switching between the open and the closed conformations, the gating helix is strictly conserved in all known monomeric Sec14 proteins and in dimeric Sfh3. This suggests that changes in α7 in the binding pocket of Sfh3 are the major contributing factors to the formation of the dimer interface. It is unclear whether the changes cause the dimerization or whether the formation of the interface forces the binding pocket to differ drastically.

Analysis of the residues in the variable regions of the binding pocket provides some insights. Fig. 4(*a*) shows substitutions of several important residues of Sfh3, including Gly220, Val221 and Gly222, which correspond to the 'bending position' in the counterpart of α7 in Sec14. According to peptide stereochemistry, the presence of glycine in an α-helix causes a negative effect because its small side chain destabilizes the α-helical conformation. Therefore, the presence of two adjacent Gly residues in Sfh3 may possibly interrupt the extension of α7, resulting in a fundamental change in the binding pocket.

In addition, we observed that residues 211–217, which closely precede Gly220, Val221 and Gly222, are disordered in the crystal structure. An interesting notion is the possibility that these disordered residues may form a helix as in other Sec14 proteins when the dimeric interaction disappears. However, the presence of three proline residues within residues 211–217, especially the contiguous Pro215 and Pro216, argues strongly against this idea (Fig. 4*b*). Proline residues disrupt α-helix formation, since their α-amino group is secondary and lacks the ability to donate a proton to α-helix hydrogen bonding. We conclude that the changes in the α7 helix, which stem from the sequence, are reflected in the secondary structure and profoundly affect the dimer interface of Sfh3.

Interestingly, Pro residues are also observed in the corresponding regions of Sfh2 and Sfh4 (Pro240 in Sfh2 and Pro211, Pro219 and Pro220 in Sfh4; Fig. 4*b*), suggesting that they cannot form an ordered α-helix either. Although structures of Sfh2 and Sfh4 are not yet available in the PDB, analysis of their sequences may suggest some structural information about the binding pockets of Sfh2 and Sfh4.

3.6. Structural basis of substrate binding

It has been shown that Sfh3 has the ability to bind PtdIns but not PtdCho (Li *et al.*, 2000). Sequence alignment indicates that the key residues for PtdIns binding are conserved in Sfh3. Docking of PtdIns into the closed Sfh3 model also exhibits a consistent result (§2.3).

As shown in Fig. 5(*a*), in Sfh1 PtdIns forms 12 pairs of hydrogen bonds (to residues Arg61, Gln204, Glu209, Arg210, Met211, Asp235, Thr238 and Lys241) which immobilize the inositol head-group. Docking studies of Sfh3 suggest that PtdIns can form the same number of hydrogen bonds to Sfh1, with most of the residues being conserved (Gln230/Gln204, Glu235/Glu209, Arg236/Arg210, Leu237/Met211, Asp261/Asp235, Thr264/Thr238 and Lys267/Lys241). One residue in Sfh1, Arg61, is replaced by Arg92 in Sfh3, a non-conserved residue from another helix (Fig. 5*b*). All of the hydrogen-bond distances, including the new pair formed by Arg92, are acceptable (2.7–3.3 Å) and no steric exclusions exist, indicating the rationality of the docking result.

However, in the Sec14 domain PtdCho binding is quite different from PtdIns binding. Previous studies of Sfh1 with PtdIns (PDB entry 3b7n) and PtdCho (PDB entry 3b7q) have revealed that the Sec14 domain uses different strategies for binding (Schaaf *et al.*, 2008). In the PtdCho–Sfh1 and PtdIns–Sfh1 complexes the phospholipid head-groups are bound at distinct sites. Using the same docking method, we did not obtain any reliable result for the closed Sfh3 model (Supplementary Figs. S5*a* and S5*b*). All of the hydrophilic residues except for the conserved residues for PtdIns binding are mutated to hydrophobic residues, including the key residues that interact with PtdCho in Sfh1 and the potential 'polar points' for contacting the substrate (Supplementary Figs. S5*c* and S5*d*). Therefore, we conclude that Sfh3 cannot supply any

effective 'polar point' for interaction with the head-group of PtdCho, which may lead to the loss of binding.

3.7. Dimer–monomer state change induced by PtdIns binding

An additional question concerns whether the structural changes in Sfh3 affect PtdIns binding. In the Sfh3 monomer the PtdIns-binding sites are not close to the changes of the pocket in space and it appears that the two parts are structurally independent. However, a connection emerged when we associated the structural changes with Sfh3 dimer formation.

In §§3.4 and 3.5, we confirmed the formation of dimeric Sfh3 *in vitro* and indicated that the changes in the pocket (α7) originating from the sequence facilitate dimerization. However, the dimeric structure of Sfh3 raises two issues concerning substrate binding which conflict with views from previous models. Firstly, the cavity of the binding pocket is not empty in dimeric Sfh3, even though Sfh3 is in an open conformation (§3.1). The gating helix from one molecule of the dimer occupies the supposed channel for phospholipid tails, thus blocking substrate cycling into and out of the interior of the pocket. Secondly, the dimeric Sfh3 structure does not fit well to the 'bulldozer' model of Sec14-mediated phospholipid exchange *in vivo*. In this model, the hydrophobic gating helix on the protein surface functions as a 'bulldozer' that drags the substrate from the binding pocket and abstracts another phospholipid from the lipid bilayer (Sha *et al.*, 1998). However, in Sfh3 the gating helix is a part of the dimer interface, which is buried within the protein interior. Thus, the gating helix cannot connect to the lipid bilayer as in monomeric Sec14 proteins. Therefore, based on the structural analysis above and the known protein-substrate binding mode in Sec14 proteins, we hypothesized that Sfh3 binding to substrates requires a monomeric state rather than a dimer.

Before discussing this idea further, we first wished to test whether dimeric Sfh3 may be in an inactive conformation owing to its recombinant expression. To determine this, isothermal titration calorimetry (ITC) was used (see Supplementary Material). An ITC assay using purified recombinant dimeric Sfh3 showed that it had significant PtdIns-binding activity (Fig. 5*c*). When we processed the data using a single-site model and calculated the concentration of Sfh3 as a monomer, the stoichiometry of the binding sites was 0.714 ± 0.156, indicating that the molecular binding ratio was close to 1:1. These results showed that the recombinant dimeric Sfh3 preserves a significant ability to bind PtdIns *in vitro*.

Following the results of the ITC assays, we further developed our hypothesis concerning PtdIns binding by Sfh3. We reasoned that a possible transformation from dimer to monomer could occur when Sfh3 binds to PtdIns. Using high-resolution FPLC size-exclusion chromatography as a molecular-mass sensor in solution, we designed a simple and effective substrate–protein incubation experiment (§2.4). Fig. 6(*a*) shows the transformation of dimeric Sfh3 to monomers after substrate incubation. The protein elutes as a new peak with an apparent size of 40 kDa from Superdex 75, which is significantly different from the peak for the dimeric Sfh3 in the absence of PtdIns used as a control.

These results show a change in the oligomeric state of Sfh3 after incubation with PtdIns. As discussed in §3.4, we confirmed that Sfh3 is stable as a

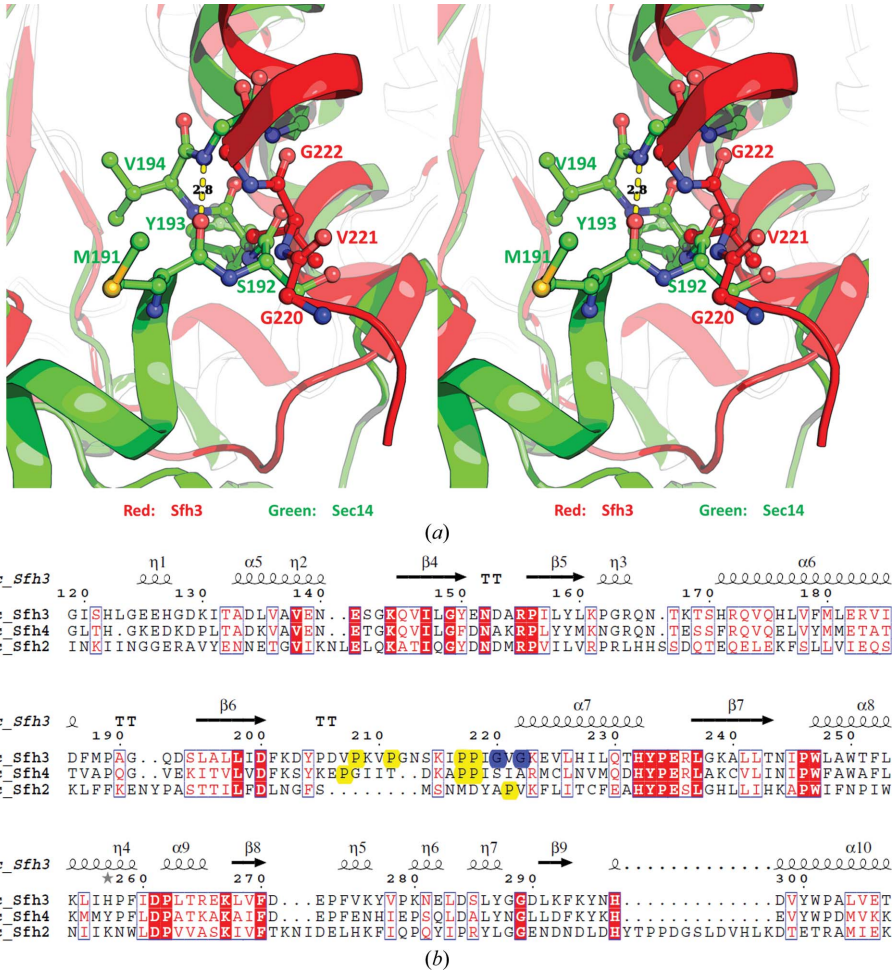

Figure 4
(*a*) Structural analysis of changes in the binding pocket of Sfh3. The red ribbon represents the structure of Sfh3 and the green ribbon represents Sec14. Some key residues (Gly220, Val221 and Gly222 in Sfh3 and Met191, Ser192, Tyr193 and Val194 in Sec14) are shown in stick form. (*b*) Structure-based sequence alignment of Sfh2, Sfh3 and Sfh4. The results are coloured by *ESPript* (http://espript.ibcp.fr/Espript/Espript). Conserved residues are shown in red and strictly conserved residues are shown on a red background. Key Pro and Gly residues are highlighted in yellow and blue, respectively.

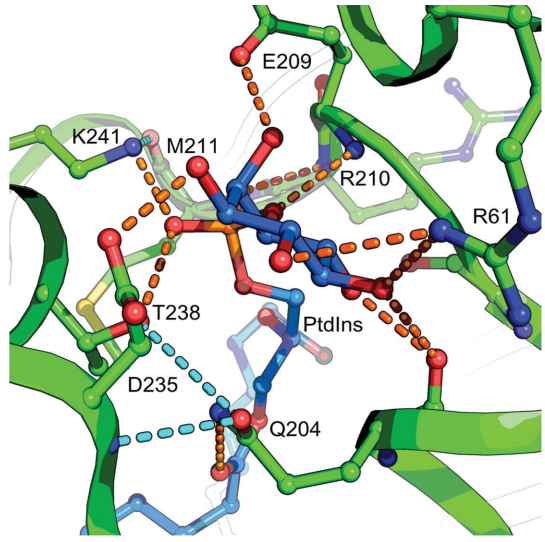

(*a*)

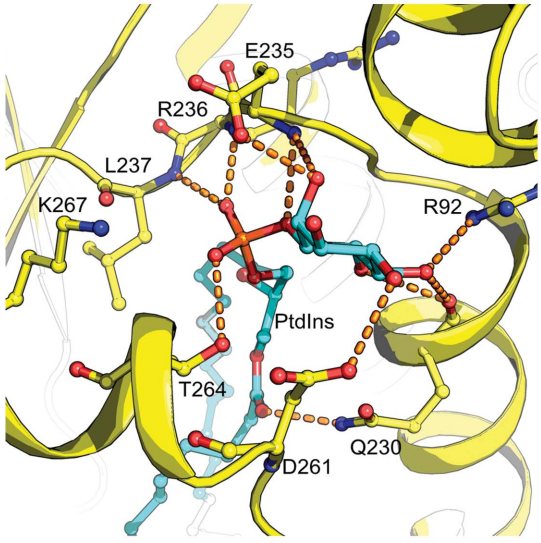

(*b*)

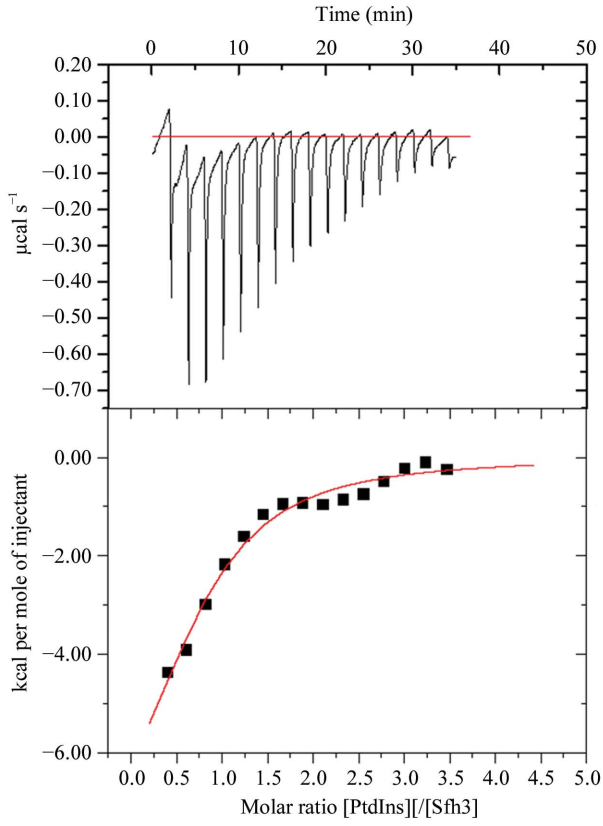

Model	ΔH (kcal mol^{-1})	ΔS (cal mol^{-1} deg^{-1})	K (M^{-1})	N
Single site	−9.31 ± 2.52	−11.2	23 400 ± 6710	0.71 ± 0.16

(*c*)

Figure 5
(*a*) Hydrogen-bonding interactions of PtdIns with Sfh1. The protein backbone is shown as a ribbon model (green) and the residues involved in the hydrogen-bonding interactions within PtdIns (blue) are displayed in stick form. (*b*) Results of the docking of PtdIns into the closed Sfh3 model. Its detailed description is similar to that in (*a*) (Sfh3 backbone in yellow and PtdIns in cyan). (*c*) Thermograms and ITC binding isotherms for the binding of PtdIns to Sfh3. The binding isotherm is normalized as kcal per mole of injectant and is plotted against the molar ratio of PtdIns to Sfh3. All data were corrected with reference to a control in which PtdIns was injected into the dialysis buffer without Sfh3. Thermodynamic parameters are tabulated in the table at the bottom.

dimer in the absence of PtdIns even at concentrations much lower (<15 µ*M*) than that used in the experiment (about 100 µ*M*; Fig. 6*b*). Thus, the dimer–monomer change cannot be the consequence of a decreased protein concentration. A possible explanation for the dimer–monomer state change is that PtdIns binding destabilizes the Sfh3 dimer, converting the dimeric Sfh3 (without PtdIns) to monomeric Sfh3 (possibly with PtdIns). Therefore, considering that changes in α7 facilitate dimerization and the phenomenon of dimer–monomer state transformation, we associate these structural changes with PtdIns binding. This association also suggests that the dimer interface of Sfh3 could form the structural basis of the dimer–monomer state transformation.

4. Conclusion

Here, we report the 2.34 Å resolution crystal structure of Sfh3, which is the first report of a dimeric Sec14 protein. Some motifs are inserted in the structure of Sfh3, and α7, which forms one side of the binding pocket, differs drastically from other Sec14-family proteins. We also identified the dimer interface of Sfh3, which may form a structural link between the dimer–monomer state transition of Sfh3 and PtdIns binding. Moreover, the change in α7 and substitutions in the residues pointing into the interior together reshape the pocket, leading to the largest volume among known Sec14 domains. These structural features show crucial differences between Sfh3 and other Sec14 proteins and will help us to

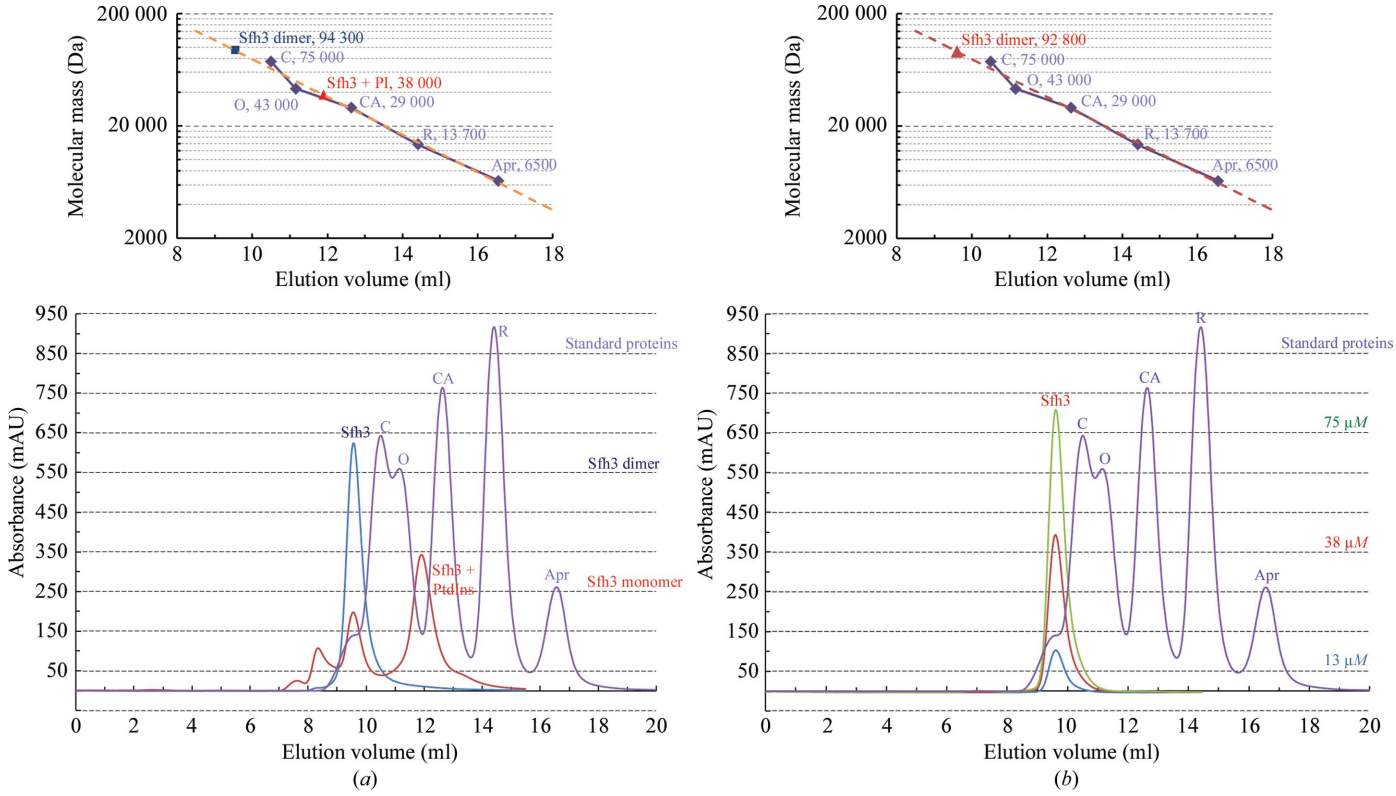

Figure 6
(*a*) The results of incubation of Sfh3 with PtdIns. The curves for Sfh3 (control) and Sfh3 with PtdIns are coloured blue and red, respectively. The top figure displays a modified calibration curve determined from five standard proteins (from Gel Filtration Calibration Kit LMW; GE Healthcare, USA) on Superdex 75 16/600 (GE Healthcare, USA): conalbumin (C, 75 000 Da), ovalbumin (O, 43 000 Da), carbonic anhydrase (CA, 29 000 Da), ribonuclease A (R, 13 700 Da) and aprotinin (Apr, 6500 Da). The elution positions of the Sfh3 dimer and the Sfh3 monomer are shown in the bottom figure and correspond to calculated molecular masses of 94.3 and 38.0 kDa, respectively. (*b*) Results of gel filtration for three Sfh3 samples at different concentrations compared with standard proteins. The detailed description of the top figure is as in (*a*). The bottom figure shows the elution profile of Sfh3 samples compared with standard proteins. The samples at 75, 38 and 13 μ*M* are coloured green, red and blue and the standard proteins are shown in purple.

understand the significance of variation in the binding pocket for substrate binding and dimerization. The features also support the hypothesis of substrate binding by Sec14 proteins (Bankaitis *et al.*, 2010) and provide some new clues for the functional study of Sfh3 and other Sec14 proteins.

We appreciate the assistance from Shanghai Synchrotron Radiation Facility (SSRF). Financial support for this project was provided by research grants from the Chinese Ministry of Science and Technology (grant Nos. 2012CB917200 and 2009CB825500) and the Chinese National Natural Science Foundation (grant Nos. 31130018 and 31170726), Natural Science Foundation of Anhui Province (grant No. 090413085) and the Junior Scientist Funds of USTC (grant No. KA207000007).

References

Adams, P. D., Grosse-Kunstleve, R. W., Hung, L.-W., Ioerger, T. R., McCoy, A. J., Moriarty, N. W., Read, R. J., Sacchettini, J. C., Sauter, N. K. & Terwilliger, T. C. (2002). *Acta Cryst.* D**58**, 1948–1954.
Bankaitis, V. A., Mousley, C. J. & Schaaf, G. (2010). *Trends Biochem. Sci.* **35**, 150–160.
Chen, V. B., Arendall, W. B., Headd, J. J., Keedy, D. A., Immormino, R. M., Kapral, G. J., Murray, L. W., Richardson, J. S. & Richardson, D. C. (2010). *Acta Cryst.* D**66**, 12–21.
Cichowski, K. & Jacks, T. (2001). *Cell*, **104**, 593–604.
Davis, I. W. & Baker, D. (2009). *J. Mol. Biol.* **385**, 381–392.
Di Paolo, G. & De Camilli, P. (2006). *Nature (London)*, **443**, 651–657.
Emsley, P. & Cowtan, K. (2004). *Acta Cryst.* D**60**, 2126–2132.
Fruman, D. A., Meyers, R. E. & Cantley, L. C. (1998). *Annu. Rev. Biochem.* **67**, 481–507.
Griac, P., Holic, R. & Tahotna, D. (2006). *Biochem. Soc. Trans.* **34**, 377–380.
Hazel, H. B. van den, Pichler, H., do Valle Matta, M. A., Leitner, E., Goffeau, A. & Daum, G. (1999). *J. Biol. Chem.* **274**, 1934–1941.
Holm, L. & Rosenström, P. (2010). *Nucleic Acids Res.* **38**, W545–W549.
Ile, K. E., Schaaf, G. & Bankaitis, V. A. (2006). *Nature Chem. Biol.* **2**, 576–583.
Kearns, B. G., McGee, T. P., Mayinger, P., Gedvilaite, A., Phillips, S. E., Kagiwada, S. & Bankaitis, V. A. (1997). *Nature (London)*, **387**, 101–105.
Krissinel, E. & Henrick, K. (2007). *J. Mol. Biol.* **372**, 774–797.
Lambert, C., Léonard, N., De Bolle, X. & Depiereux, E. (2002). *Bioinformatics*, **18**, 1250–1256.
Leaver-Fay, A. *et al.* (2011). *Methods Enzymol.* **487**, 545–574.
Leite, T. B., Gomes, D., Miteva, M. A., Chomilier, J., Villoutreix, B. O. & Tufféry, P. (2007). *Nucleic Acids Res.* **35**, W568–W572.

Lemmon, M. A. (2008). *Nature Rev. Mol. Cell Biol.* **9**, 26–111.
Li, X., Routt, S. M., Xie, Z., Cui, X., Fang, M., Kearns, M. A., Bard, M., Kirsch, D. R. & Bankaitis, V. A. (2000). *Mol. Biol. Cell*, **11**, 1989–2005.
Maw, M. A., Kennedy, B., Knight, A., Bridges, R., Roth, K. E., Mani, E. J., Mukkadan, J. K., Nancarrow, D., Crabb, J. W. & Denton, M. J. (1997). *Nature Genet.* **17**, 198–200.
Meier, R., Tomizaki, T., Schulze-Briese, C., Baumann, U. & Stocker, A. (2003). *J. Mol. Biol.* **331**, 725–734.
Murshudov, G. N., Skubák, P., Lebedev, A. A., Pannu, N. S., Steiner, R. A., Nicholls, R. A., Winn, M. D., Long, F. & Vagin, A. A. (2011). *Acta Cryst.* D**67**, 355–367.
O'Boyle, N. M., Banck, M., James, C. A., Morley, C., Vandermeersch, T. & Hutchison, G. R. (2011). *J. Cheminform.* **3**, 33.
Otwinowski, Z. & Minor, W. (1997). *Methods Enzymol.* **276**, 307–326.
Ouachi, K. *et al.* (1995). *Nature Genet.* **9**, 141–145.
Phillips, S. E., Vincent, P., Rizzieri, K., Schaaf, G., Gaucher, E. A. & Bankaitis, V. A. (2006). *Crit. Rev. Biochem. Mol. Biol.* **41**, 1–28.
Ryan, M. M., Temple, B. R., Phillips, S. E. & Bankaitis, V. A. (2007). *Mol. Biol. Cell*, **18**, 1928–1942.
Salama, S. R., Cleves, A. E., Malehorn, D. E., Whitters, E. A. & Bankaitis, V. A. (1990). *J. Bacteriol.* **172**, 4510–4521.
Schaaf, G., Dynowski, M., Mousley, C. J., Shah, S. D., Yuan, P., Winklbauer, E. M., de Campos, M. K. F., Trettin, K., Quinones, M., Smirnova, T. I., Yanagisawa, L. L., Ortlund, E. A. & Bankaitis, V. A. (2011). *Mol. Biol. Cell*, **22**, 892–905.
Schaaf, G., Ortlund, E. A., Tyeryar, K. R., Mousley, C. J., Ile, K. E., Garrett, T. A., Ren, J., Woolls, M. J., Raetz, C. R., Redinbo, M. R. & Bankaitis, V. A. (2008). *Mol. Cell*, **29**, 191–206.
Schnabl, M., Oskolkova, O. V., Holic, R., Brezná, B., Pichler, H., Zágorsek, M., Kohlwein, S. D., Paltauf, F., Daum, G. & Griac, P. (2003). *Eur. J. Biochem.* **270**, 3133–3145.
Sha, B., Phillips, S. E., Bankaitis, V. A. & Luo, M. (1998). *Nature (London)*, **391**, 506–510.
Singer, S. J. & Nicolson, G. L. (1972). *Science*, **175**, 720–731.
Stocker, A., Tomizaki, T., Schulze-Briese, C. & Baumann, U. (2002). *Structure*, **10**, 1533–1540.
Strahl, T. & Thorner, J. (2007). *Biochim. Biophys. Acta*, **1771**, 353–404.
Voss, N. R. & Gerstein, M. (2010). *Nucleic Acids Res.* **38**, W555–W562.
Wallace, A. C., Laskowski, R. A. & Thornton, J. M. (1996). *Protein Eng.* **8**, 127–134.
Walsh, M. A., Dementieva, I., Evans, G., Sanishvili, R. & Joachimiak, A. (1999). *Acta Cryst.* D**55**, 1168–1173.
Welti, S., Fraterman, S., D'Angelo, I., Wilm, M. & Scheffzek, K. (2007). *J. Mol. Biol.* **366**, 551–562.
Ye, Y. & Godzik, A. (2003). *Bioinformatics*, **19**, ii246–ii255.